24th COBEM - 2017

24th ABCM International Congress of Mechanical Engineering
December 3-8, 2017, Curitiba, PR, Brazil

COBEM-2017- 1003
CFD STUDY ON THE INFLUENCE OF FREE SURFACE AND TURBULENCE MODELING ON THE FLOW AROUND A FIXED CIRCULAR CYLINDER WITH LOW ASPECT RATIO

Pedro Paludetto Silva de Paula Lopes
University of São Paulo, Escola Politécnica, São Paulo, SP, Brazil
pedropaludetto@usp.br

Guilherme Feitosa Rosetti
Argonáutica Engineering and Research, São Paulo, SP, Brazil
rosetti@argonautica.com.br

Celso Pupo Pesce
Offshore Mechanics Laboratory, Universisty of São Paulo, Escola Politécnica, São Paulo, SP, Brazil
ceppesce@usp.br

Rodolfo Trentin Gonçalves
The University of Tokyo, Dept. of Ocean Technology, Policy, and Environment, Kashiwa-shi, Chiba, Japan
goncalves@edu.k.u-tokyo.ac.jp

Abstract. *Offshore multi-column platforms as semi-submersibles (SS) and floating offshore wind turbines (FOWT) are ocean structures composed of a set of free surface piercing low aspect ratio (LAR) vertical circular cylinders. Under ocean current, vortex shedding phenomena take place, inducing what has been called Vortex Induced Motions (VIM). Fundamental studies on the vortex shedding phenomenon from LAR cylinders are still required. This paper brings a study on the influence of the boundary conditions and two different turbulence models on the flow and the drag coefficient. The model is constructed with the Star CCM® solver. The unsteady incompressible URANS (Unsteady Reynolds-Averaged Navier-Stokes) equations are dealt with a k-ω SST turbulence model (Shear Stress Transport) and DES turbulence model (Detached Eddy Simulation).*

Keywords: *CFD, Free-Surface, Low Aspect-Ratio Cylinder, Turbulence Model, VIM.*

1. INTRODUCTION

The flow around low-aspect-ratio cylinders piercing the free surface is a source of considerable industrial and academic interest. Several engineering applications feature low aspect ratio (LAR) cylindrical shapes as part of their geometry, such as in offshore floating platforms, spars, monocolumns, semi-submersibles (SS) and FOWT - floating offshore wind turbines. The typical flow exhibits a complex vortex system, interacting with the free-surface and with the free end of the column, in a three-dimensional way, what represents a challenge to experimental and numerical engineering.

Fujarra *et al.* (2012) present some VIM experiments, indicating that, initially, research in this theme focused more on faithful reproduction of the main features, in small-scale models, rather than on the global understanding of the phenomena.

Fundamental studies about the vortex flow topology around LAR cylinders were carried out by Okamoto and Yagita (1973), Kawamura *et al.* (1984), Sakamoto and Arie (1983) and Pattenden et al. (2005). Sakamoto and Pattenden classified vortices shedding from LAR cylinders as a tip and trailing vortices. Okamoto and Kawamura conducted experimental tests of cylinders varying the aspect ratio (AR) from 1 to 8 and analyzed the influence of free-end effects on drag coefficient. More recently, Gonçalves *et al.* (2014, 2015) carried out an extensive series of experiments on flow around fixed LAR circular cylinders and VIM tests of floating LAR circular cylinders, both covering the range $0.2 \leq AR \leq 2.0$.

Rosetti et al. (2013), conducted a numerical verification study for a free surface piercing low aspect ratio circular cylinder, AR=2.0, comparing the solution with experimental results. In Lopes *et al.* (2017), a CFD study with circular,

square and diamond shaped cylinders (AR=1.5), at Re~10^5 was done. Palau-Salvador *et al.* (2010) presented a comparison between numerical and experimental results using LES (Large Eddy Simulations) for a cylinder with AR 2.5 and 5. Benitz et al. (2016) carried out an extensive numerical simulation for LAR cylinders, varying AR in the range 1 to 19, applying several turbulence models (Spalart-Allmaras, k-ε, RNG, and DES) and analyzed the influence of free-end and free-surface effects.

The objective of the present paper is to understand the influence of the free surface and turbulent fields on the flow around a fixed column for Reynolds 25,000 and Froude number 0.18, both based on flow velocity and cylinder diameter. The results are compared with experimental fields obtained by PIV by Gonçalves et al. (2013), as well compared with numerical fields obtained by Rosetti *et al.* Besides, the mean drag coefficient is addressed.

The paper is organized as follows: after this introduction, the formulations used for the URANS code are briefly explained. The numerical setup and simulation conditions are then explained in detail, followed by a qualitative analysis of the obtained flow fields. A comparison between numerical and experimental results is presented in the following section. The last section presents the conclusions.

2. THEORETICAL FORMULATIONS

The flow governing equations are the unsteady Reynolds averaged Navier-Stokes equations, written in an inertial fixed reference frame (x_1, x_2, x_3) = (x, y, z), for Newtonian fluids in incompressible flow; see for instance Ferziger and Peric (2002):

$$\frac{\partial(\rho Ui)}{\partial t} + \frac{\partial}{\partial xj}\left(\rho U_i U_j + \rho\overline{u'_i u'_j}\right) == -\frac{\partial P}{\partial x_i} + \frac{\partial}{\partial x_j}\left[\mu\left(\frac{\partial U_i}{\partial x_j} + \frac{\partial U_j}{\partial x_i}\right)\right] + \rho B_i \tag{1}$$

$$\frac{\partial(\rho Ui)}{\partial x_i} = 0 \tag{2}$$

where ρBi is a body force (ρ is the mass density). U_i is the velocity field on i direction and μ is the dynamic viscosity. The correlations $\overline{u'_i u'_j}$ cannot be determined without further equations. In URANS framework, one normally employs turbulence models to determine these correlations.

In the case of free surface flows, a few further assumptions are made. Part of the body force present in Eq.1 is the gravitational force, i.e., $\rho B_i = \rho g_i$. The fluid is considered as a two-phase fluid mixture according to the volume-of-fraction (VoF) approach, in which density and viscosity are space and time-varying properties:

$$\rho = \alpha_w \rho_w + \alpha_a \rho_a \tag{3}$$

$$\mu = \alpha_w \mu_w + \alpha_a \mu_a \tag{4}$$

where α_w is the volume fraction occupied by water in the field and α_a, by air. Moreover, ρ_w, ρ_a, μ_w, and μ_a are, respectively, water and air densities and water and air viscosities. Therefore the following applies in an arbitrary control volume V:

$$\alpha_w = \frac{V_w}{V} \tag{5}$$

$$\alpha_a = \frac{V_a}{V} \tag{6}$$

$$\alpha_w + \alpha_a = 1 \tag{7}$$

With such an explicit relation for the volume fractions, we are then able to solve for only one of them and the other results automatically. It is also worth emphasizing that it follows from the equations that $0 \leq \alpha \leq 1$. The turbulence models applied to the calculations are kω-SST, Detached Eddy Simulation (DES) and Spalart-Allmaras.

3. NUMERICAL SETUP

In this section, we address grids, boundary conditions and numerical convergence aspects.

3.1 Domain and Grids

In all cases, the domain was placed 10 diameters upstream and 20 diameters downstream the cylinder. The walls of the domain and the depth were modeling according to the dimensions of the NDF recirculating water channel facility of

the University of São Paulo (USP) where the experimental data [5] and [6] were obtained. Two types of boundary conditions are addressed. The first one replaces the free surface by a symmetric boundary condition, simply referred to as *Symmetry*. The second one represents the kinematic and dynamic boundary conditions, simply referred to as Free Surface (FS) or VoF. The second case is simulated using kω-SST, DES and Spalart-Allmaras turbulence models.

3.1.1 Symmetry

In this setup, the objective is to investigate the free-end influences with no the free surface effect. The domain and grid can be seen in Fig.1.

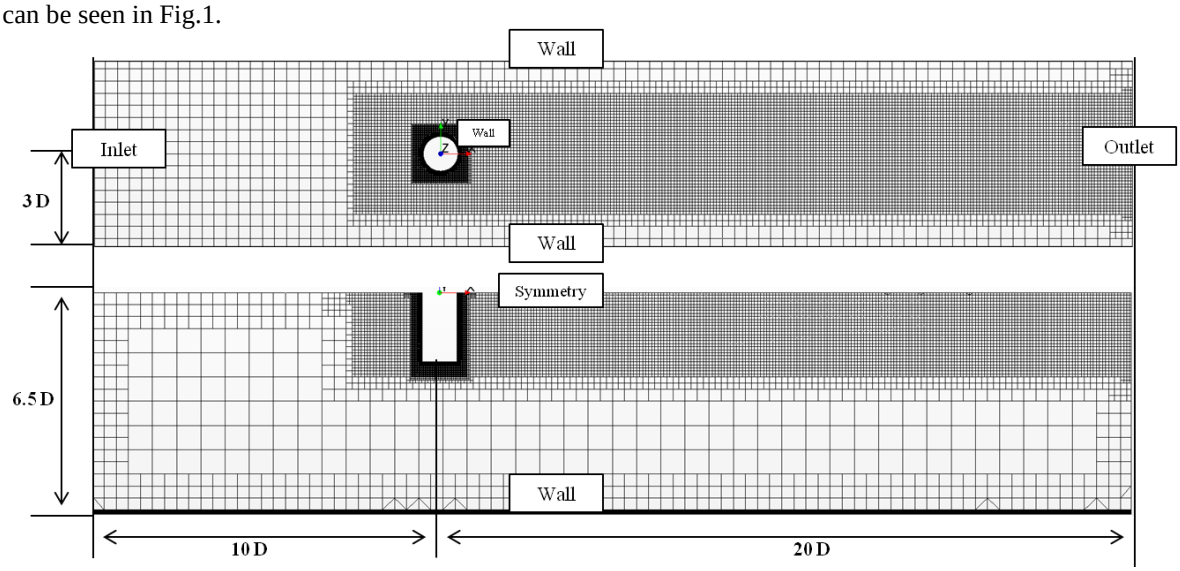

Figure 1. Grid and boundary conditions for the symmetry case.

The grid has 1.6 M cells. The boundary layer region was refined and the first layer thickness selected to keep $Y^+<1$.

3.1.2 Free surface effects - VoF

The objective of this case is investigating the free surface effects and turbulence modeling effects. The domain and grid can be seen in Fig.2. Slices shown in Fig. 2 are in the free-surface plane.

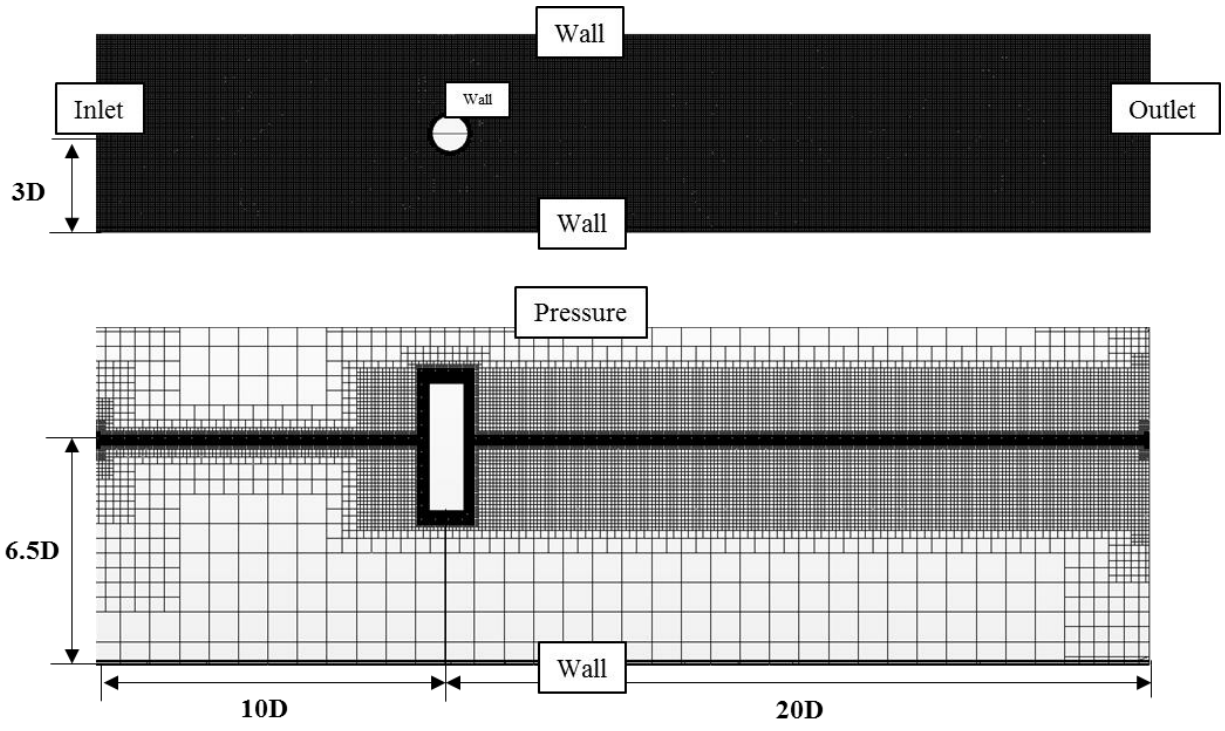

Figure 2. Grid and boundary conditions for the symmetry boundary condition.

This case is what best represents the experiments. The numbers of cells increases to 5.3 million elements. The boundary layer refinement in this case also was set to keep $y+$ below 1. The refinement blocks for this case were set in three regions. The region near to the cylinder, to make the transition between the boundary layer and far-field smoothest. The second region is the wake region, and finally the free surface region, which represents the volumetric interface between water and air. This region must be the most refined compared to the other two to mitigate errors by numerical diffusion.

3.2 Boundary Conditions

At the inlet boundary, velocity field and turbulent quantities distribution are specified as Dirichlet boundary conditions. The volume fraction is also defined by specifying the position of the air-water interface. On the outlet boundary, a boundary condition of zeroth-order extrapolates all quantities, except the pressure, which is fixed. Such a condition is also used on the top of the domain in the free surface case.

The non-slip condition is applied on the surfaces of the walls, bottom, and cylinder.

For the symmetry case, a symmetry boundary condition was applied to the still free surface plane. In this case, the normal component of the velocity and the gradient of the tangential component of the velocity are set to zero (mixed Dirichlet-Neumann conditions). For other quantities, there should be a Neumann condition (zero gradients).

3.3 Iterative Convergence

The criteria for the iterative errors in the calculations for all variables was set to residual $<10^{-4}$ at each time-step in the rms norm. Fig. 3 shows an example of the iterative convergence process.

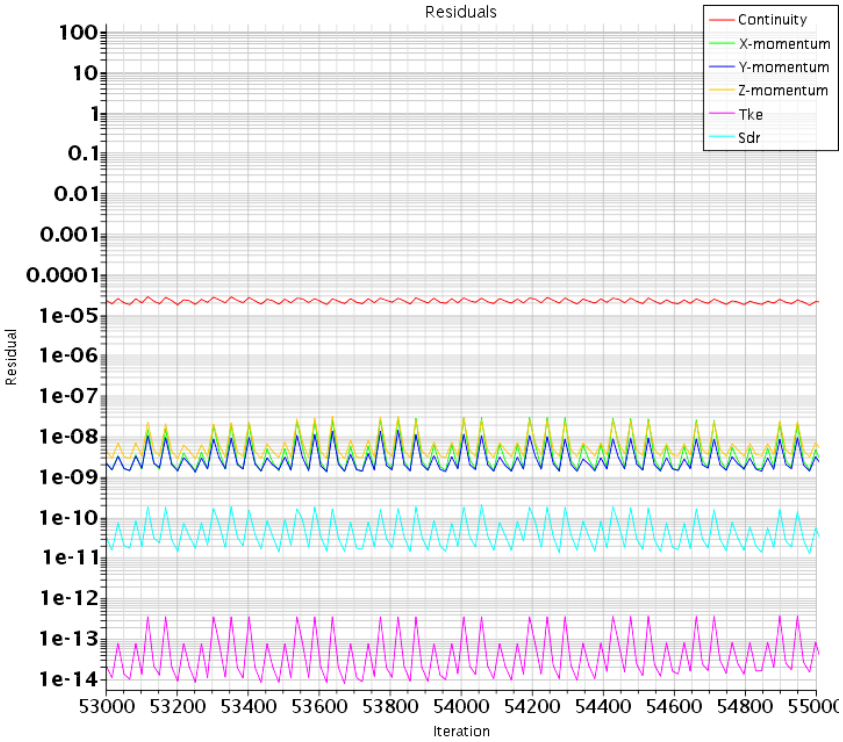

Figure 3. Example of the iterative convergence.

4. PRELIMINARY RESULTS

In this section, some results are shown and compared with numerical ones, by Rosetti *et al.* (2013), and with experimental ones, by Gonçalves *et al.* (2013, 2015). Drag coefficient and flow fields are considered.

4.1 Drag coefficient.

The mean drag coefficient is determined for each case simulated, after identifying steady-state regimes. The drag coefficient is defined by considering the frontal projected area of the cylinder (*HD*).

Table 1 shows a comparison between the mean drag coefficient, determined from the three cases simulated, with experimental results by Gonçalves *et al.* (2013, 2015) and with numerical results obtained by Rosetti *et al.* (2013).

Table 1. Mean drag coefficient (C_x): comparison between numerical and experimental results.

Case	C_x	Relative difference (%) Experimental	Relative difference (%) Numerical (Kω-SST + Symmetry)
Gonçalves et al, 2013 (Experimental)	1.02	-	
Rosetti *et al.* (2013) (Kω-SST + Symmetry)	0.74	27.5%	-
Rosetti *et al.* (2013) (Kω-SST + Free Surface)	0.82	19.5%	11.1%
Kω-SST + Symmetry	0.75	26.6%	1.3%
Kω-SST + Free surface	0.85	16.9%	14.7%
DES + Free surface	0.89	12.5%	20.8%
Spalart-Allmaras + Free surface	0.73	28.4%	1.2%

As can be noticed, the simulation cases which best reproduce the experimental results are those with free-surface modeling. Between those, the one that gives a value closer to the experimental paradigm is that with DES turbulence model. If we compare with the numerical results by Rosetti *et al.* (2013), the relative difference of the simulations using the Kω-SST + Symmetry model are of the order of 1%.

4.2 Velocity Flow Fields

In this section, we compare some obtained flow fields with experimental data from PIV (Particle Image Velocimetry) by Gonçalves *et al.* (2013) and with previous numerical results by Rosetti *et al.* (2013).

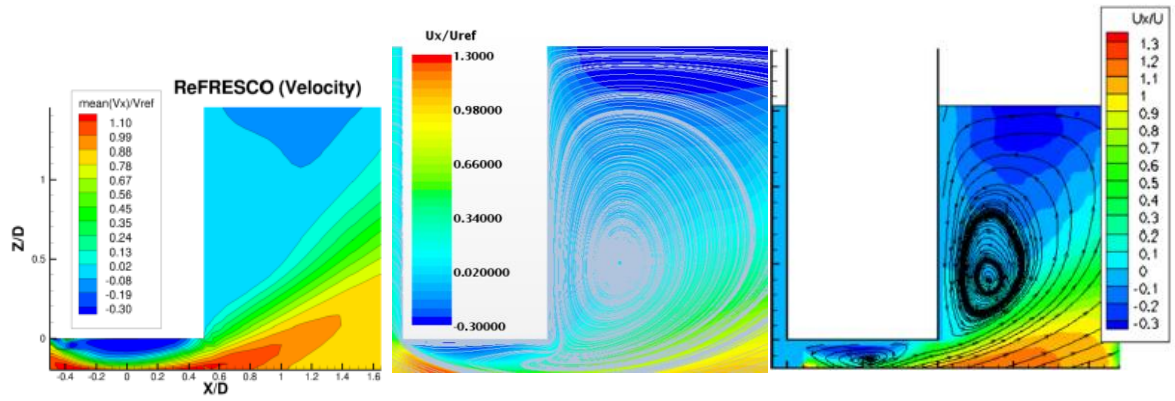

(a) (b) (c)

Figure 4. Mean velocity in the *x*-direction; kω-SST turbulence model and symmetry boundary condition. a) Numerical results, Rosetti *et al.* (2013); b) Numerical results, present work; c) Experimental PIV results, Gonçalves *et al.* (2013). Streamlines at central plane shown in (b) and (c)

Figure 4 shows the mean velocity fields color maps in the *x*-direction, normalized by the free stream current velocity. The region very close to the free surface is not shown in the experimental results, Fig. 4-c. In the experimental results, we can see two recirculating regions, one near to the bottom of the cylinder (free-end) and another downstream. For the kω-SST turbulence model under symmetry boundary condition (Fig.4-b), the first recirculation region appears to be not reproduced. However, in the downstream region, the recirculating bubble seems similar to the experimental results.

Figure 5 shows the influence of the free surface modeling on the downstream wake. Streamlines are presented for two free surface modeling strategies.

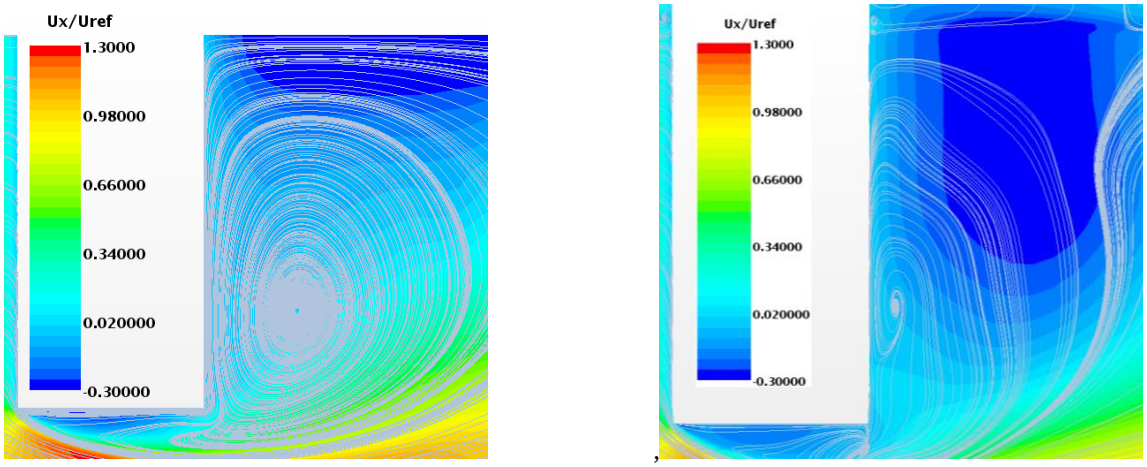

(a) (b)

Figure 5. Mean velocity in the *x*-direction; kω-SST turbulence model.
a) Symmetry boundary condition. b) Free surface modeling (VoF).
Streamlines at central plane shown.

We compare two models: symmetry and with free surface. The dimensionless velocity field was compared taking the symmetry BC case and the free surface model, both using the kω-SST turbulence model. In the VoF modeling case (Fig. 5-b), the low-velocity field region downstream is larger than in the symmetry BC case (Fig. 5-a). Close to the bottom of the cylinder, the free surface BC simulation also shows a larger low-velocity field region. Regarding streamlines, some morphologic deformation in the downstream wake can be observed from the VoF model.

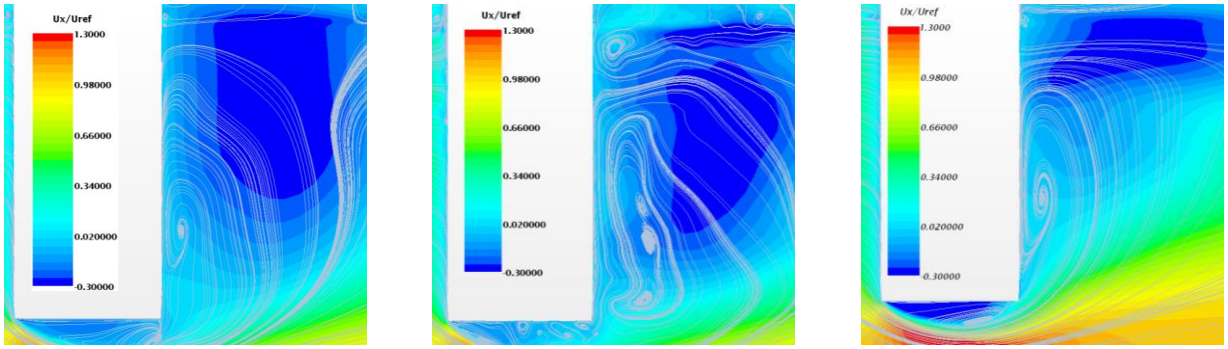

(a) (b) (c)

Figure 6. Mean velocity in *x*-direction; free surface models: a) kω-SST turbulence model; b) DES turbulence model; c) Spalart-Allmaras turbulence model. Streamlines at central plane shown.

Figure 6 aims at illustrating the influence of turbulence models on the simulations. The comparison is made only with cases considering free surface effects. The *x*-velocity field from the DES model (Fig. 6-b) shows a certain degree of non-uniformity if compared with the other two. A region near the free surface, where the velocity intensity is high, may be observed, driving a negative recirculation region near the cylinder.

5. CONCLUSIONS

Numerical simulations were carried out for the flow around a vertical captive cylinder, with the low-aspect ratio (AR=2), aiming at investigating the physics of the flow under distinct modeling strategies, particularly on the possible influence of the free surface and distinct turbulence models.

Four models were considered, contrasting results from different combinations of free surface and turbulence models. Firstly, mean drag coefficients were compared with experimental and numerical results. The comparison with experimental results showed the free surface - DES turbulence model as the one presenting the lowest relative difference, of circa 13%. The largest difference was obtained with the free surface - Spalart-Allmaras turbulence model. If compared with other numerical results, the kω-SST - symmetry model presented a deviation of 1.3%, whereas the free surface -Spalart-Allmaras model, 1.2%.

The fields are shown in three steps, first a direct comparison with experimental and numerical data from other authors. The downstream recirculating bubble appears with some similarity to the experimental results. For this model,

the recirculating bubble at the cylinder bottom region could not be properly reproduced. In a second step, velocity fields were compared taking the same turbulence model, the kω-SST, for both VoF and symmetry BCs free surface modeling. Finally, considering only the free surface BC model, velocity fields were compared, taking three turbulence modeling strategies, kω-SST, DES and Spalart-Allmaras. The DES model produced a mean *x*-velocity field with a certain degree of non-uniformity if compared with kω-SST or Spalart-Allmaras procedures. A small negative recirculating bubble downstream of the cylinder appears, near to the free surface region. Subsequent work will readdress numerical simulations closer, measuring uncertainties and applying validation and verification (V&V) procedures.

6. ACKNOWLEDGEMENTS

Authors thank the Numerical Offshore Tank Laboratory (TPN), University of São Paulo, for the use of the cluster. A PPGEN – Graduate Program in Naval and Ocean Engineering - CAPES MSc scholarship and a CNPq research grant, n. 308990/2014-5, are acknowledged.

7. REFERENCES

Benitz, M. A., Carlson, D. W., Seyed-Aghazadeh, B., Modarres-Sadeghi, Y., Lackner, M. A., Schmidt, D. P. 2016. "CFD simulations and experimental measurements of flow past free-surface piercing, finite length cylinders with varying aspect ratios". *Computers & Fluids*, Vol. 136, p. 247-259.

Ferziger, J. H., and Peric, M. 2012."*Computational methods for fluid dynamics*." Springer Science & Business Media.

Fujarra, A.L.C., Rosetti, G.F., Wilde J., Goncalves, R.T., 2012. "State-of-Art on vorte*x*-induced motion: A comprehensive survey after more than one decade of experimental investigation". In *Proceedings of the ASME2012 31st International Conference on Ocean, Offshore and Arctic Engineering - OMAE2012-83561*. Rio de Janeiro, Brazil.

Gonçalves, R. T., Franzini, G.R., Rosetti, G.F., Meneghini, J.R., Fujarra, A.L.C., 2015. "Flow around circular cylinders with very low aspect ratio". *Journal of Fluids and Structures*, Vol. 54, p. 122-141.

Gonçalves, R.T., Fujarra, A.L.C., 2014. "Experimental study on vorte*x*-induced vibration of floating circular cylinders with low aspect ratio". In *Proceedings of the ASME 2014 33rd International Conference on Ocean, Offshore and Arctic Engineering - OMAE2014-23383*. San Francisco, CA, USA.

Gonçalves, R. T. 2012. "Vibrações induzidas pela emissão de vórtices em cilindros com baixa razão de aspecto" (Doctoral dissertation, Universidade de São Paulo).

Kawamura, H., and Miyashita, S., 1984. "Phase transition of the two-dimensional Heisenberg antiferromagnet on the triangular lattice". *Journal of the Physical Society of Japan*, Vol. 53, p. 4138-4154.

Lopes, P.P.S.P., Rosetti, G.F., Hannes, N., Chame, M.E.F., Hirabayashi, H., Suzuki, H., Gonçalves, R.T., 2017. "CFD evaluation and experimental comparison on flow around fixed multi-column configurations, Part II: V&V of flow around single cylinders". in *Annual Spring Meeting of JASNAOE 2017*. Tokyo, Japan.

Okamoto, T., and Yagita, M. 1973. "The experimental investigation on the flow past a circular cylinder of finite length placed normal to the plane surface in a uniform stream". *Bulletin of JSME*, Vol. 16(95), p. 805-814.

Palau-Salvador, G., Stoesser, T., Fröhlich, J., Kappler, M., Rodi, W. 2010. "Large eddy simulations and experiments of flow around finite-height cylinders". *Flow, turbulence and combustion*, Vol. 84(2), p. 239-275.

Pattenden, R. J., Turnock, S. R., Zhang, X., 2005. "Measurements of the flow over a low-aspect-ratio cylinder mounted on a ground plane". *Experiments in Fluids*, *39*(1), 10-21.

Rosetti, G.F., Vaz, G., Hoekstra, M., Gonçalves, R.T., Fujarra, A.L.C., 2013. "CFD calculations for a free-surface-piercing low aspect ratio circular cylinder with solution verification and comparison with experiments". In *Proceedings of the ASME 2013 32nd International Conference on Ocean, Offshore and Arctic Engineering. American Society of Mechanical Engineers - OMAE2013-10963*. Nantes, France.

Sakamoto, H., and Arie, M., 1983. "Vortex shedding from a rectangular prism and a circular cylinder placed vertically in a turbulent boundary layer". *Journal of Fluid Mechanics*, Vol. 126, p. 147-165.

8. RESPONSIBILITY NOTICE

The authors are the only responsible for the printed material included in this paper.